Chapter 16
Studies on Modeling of Dynamic Compaction in a Geocentrifuge

B. V. S. Viswanadham and Saptarshi Kundu

16.1 Introduction

The engineering properties of various problematic soils, fills and waste materials existing in the field need to be improved prior to their use as construction sites and their exposure to various loading conditions. The problematic sites encountered in the field involve weak compressible soils, collapsible soils, expansive soils, fills, MSW materials, fly ash/coal ash deposits, etc. The selection of a particular improvement method depends on the type and degree of improvement required and the soil type. The standard ground improvement methods adopted in the field can be broadly classified as reinforcement techniques, densification techniques, grouting/mixing techniques and drainage techniques. Dynamic compaction (DC) is one of the most widely adopted densification techniques for geomaterials in view of its simplicity, cost-effectiveness and ease of implementation (Menard and Broise 1975; Leonards et al. 1980; Mayne et al. 1984; Lukas 1986; Rollins and Rogers 1994). The technique, also referred to as impact densification and heavy tamping, has evolved as a routine method of site improvement for treating poor soils in situ. Densification by DC is performed by dropping a heavy tamper of steel or concrete in a grid pattern from heights of 5–30 m. Liquefaction is initiated locally beneath the drop point making it easier for the sand grains to densify. When the excess pore water pressure from dynamic loading dissipates, additional densification occurs. The process is usually repeated in several passes until the required post-treatment density is achieved.

B. V. S. Viswanadham (✉) · S. Kundu
Department of Civil Engineering, Indian Institute of Technology Bombay, Mumbai 400076, India
e-mail: viswam@civil.iitb.ac.in

© The Author(s), under exclusive license to Springer Nature Singapore Pte Ltd. 2021

T. G. Sitharam et al. (eds.), *Latest Developments in Geotechnical Earthquake Engineering and Soil Dynamics*, Springer Transactions in Civil and Environmental Engineering, https://doi.org/10.1007/978-981-16-1468-2_16

Numerous studies have been reported in the literature on DC being applied on diverse geomaterials (Mayne and Jones 1983; Lutenegger 1986; Zou et al. 2005; Bo et al. 2009; Feng et al. 2011; Zekkos et al. 2013; Kundu and Viswanadham 2018, 2020). The effectiveness of DC in the context of remediation of loose soil deposits is hereby illustrated in Fig.16.1a–d. Figure 16.1a depicts the problems encountered in loose subsoils, wherein superstructure load from adjacent infrastructural facilities results in large differential settlements of the foundation and subsequent instability of the building. Figure 16.1b, c presents two alternatives in this regard, in the form of installation of conventional pile foundations and adoption of DC for soil densification, respectively. The resultant improvement achieved using DC is presented in Fig. 16.1d, wherein reduced settlements and enhanced stability to superstructure loads can be observed in the soil stratum densified by DC.

DC possesses a number of advantages compared to other ground improvement methods. DC has been successfully applied over a range of soil types, including loose granular deposits, saturated clayey soils, MSW, rockfills and mine spoils. As per the compilation of Yee and Ooi (2010), DC has the third least CO_2 emission as a ground improvement method after vacuum consolidation and vertical drain installations. Furthermore, as per the database of Geotechnical Engineering Circular No. 1 prepared by Lukas (1995) (Table 16.1), the cost for executing DC in the field is significantly less compared to other ground remediation methodologies.

During DC, the blow energy is applied in single or multiple passes in a grid pattern over the entire area. In the first stage, the blows are spaced at a distance dictated by the depth of the compressible layer, the depth of existing groundwater table and the grain size distribution of soil. Initial grid spacing is usually at least equal to the thickness of the compressible layer, and 6–50 tamper drops are imparted at each point. This first phase of the treatment with widely spaced blows is designed to improve the deeper layers. In saturated fine-grained soils, a sufficient time interval is planned between succeeding passes to allow the excess pore water pressure to dissipate. After each pass, backfilling is done periodically with surrounding materials available at the site. The initial passes are also called 'high-energy pass,' as the tamper energy is higher than subsequent passes. The second pass is generally made at the centroid points of the first pass and consists of several tamper drops at the same point, which lead to closure of the voids for achieving minimum void ratio. Finally, an 'ironing' pass with a low-energy blow and reduced drop height is performed to compact shallow soil layers. The field procedure of DC as discussed is shown in Fig. 16.2.

16.2 Scaling Considerations of DC

Physical modeling of geotechnical engineering problems can be executed at full-scale level or as a reduced scale model to replicate various field situations. However, a limitation of small-scale laboratory models under normal gravity is that the stress levels are much smaller than in prototype structures. Only full-scale

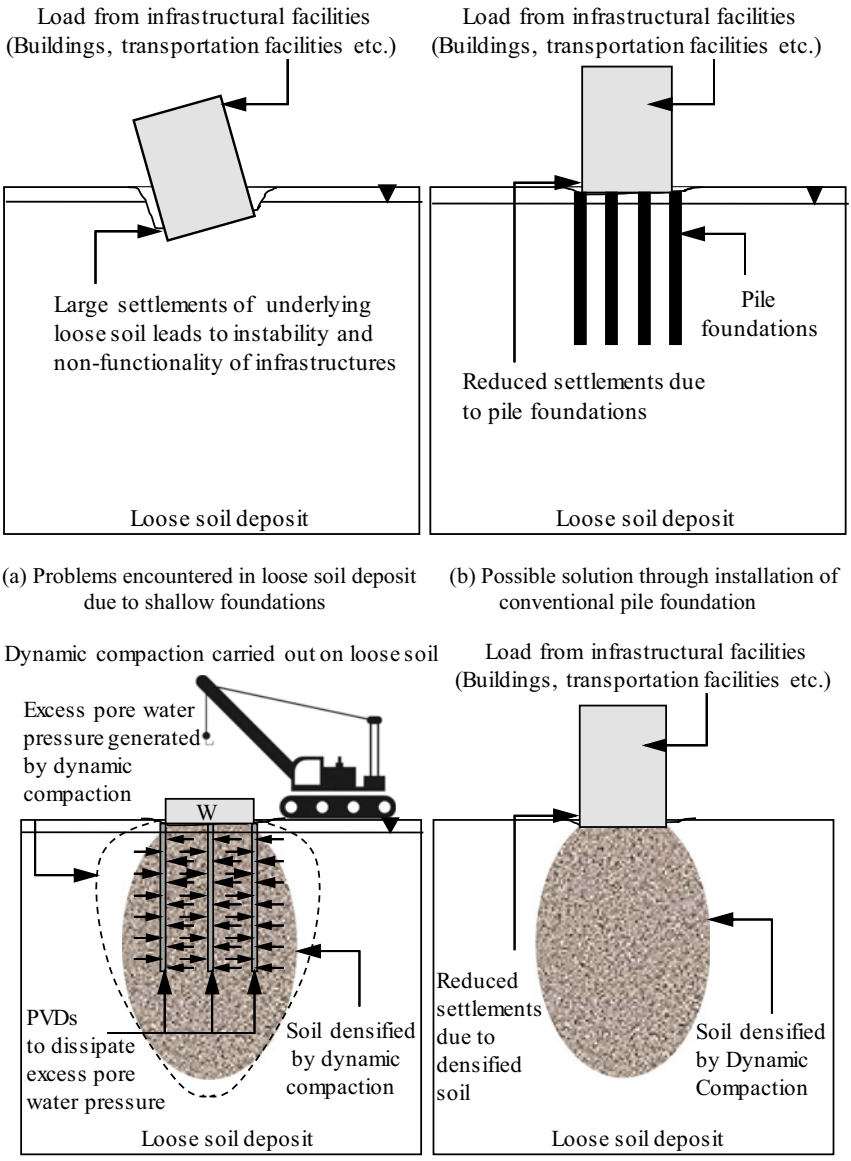

(a) Problems encountered in loose soil deposit due to shallow foundations

(b) Possible solution through installation of conventional pile foundation

(c) Alternative solution attained through densification of loose soils by DC

(d) Effective ground remediation induced by DC

Fig. 16.1 Effectiveness of DC as a ground remediation technique for geomaterials

Table 16.1 Comparative cost of different ground improvement techniques [based on the compilation of Lukas (1995)]

Treatment method	Basis of cost calculation		
	Volume of treated soil (US$/m^3)	Surface (US$/m^2)	Length (US$/m)
[a]Dynamic compaction	0.7–3	4.3–22	–
Vibro-replacement	4–12	–	30–52
Vibro-compaction	1–7	–	16–39
Excavate–replace	10–20	–	–
Slurry grouting	40–80	–	–
Chemical grouting	160–525	–	–
Compaction grouting	30–200	–	–
Jet grouting	100–400	–	82–325
[b]Freezing	275–650	110–160	–

[a]Estimate is prepared based on projects undertaken during 1985–1993
[b]Plus $2–$10.75 per sq-m/week for maintaining frozen zones

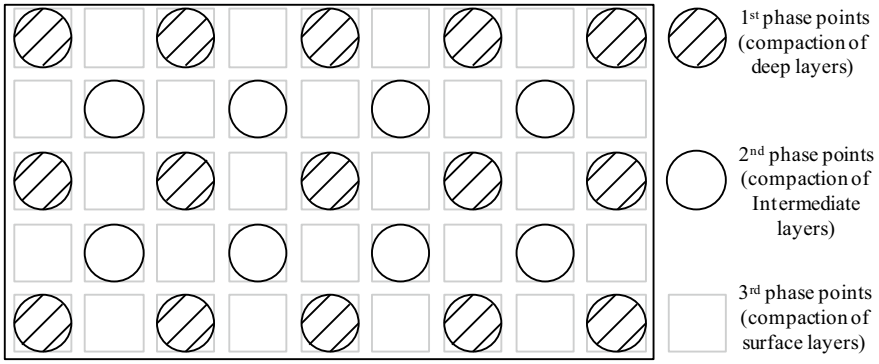

Fig. 16.2 Typical phases involved in the field during DC process

physical models can include all these complexities, but they are expensive, time-consuming and difficult to replicate with dynamic loadings similar to earthquakes, DC, blasting, etc. In such situations, geotechnical centrifuge modeling can be used as an effective tool to replicate identical stress–strain response in the model as that of the prototype (Schofield 1980; Taylor 1995; Madabhushi 2014). This enables study of the behavior of engineered earth structures in a controlled environment by deriving standard scaling laws linking the model behavior to that of corresponding prototype. The main governing parameters for modeling DC in a geocentrifuge include scaling of the mass of tamper, height of fall and frequency of

tamper drops. Considering a soil deposit of thickness d_p in the field and corresponding centrifuge model (Ng model) of thickness d_m, the relevant scaling law is presented in Eq. (16.1):

$$d_m = \frac{d_p}{N} \tag{16.1}$$

where the notations p and m are used to denote the prototype and model, respectively, and N indicates the gravity level or scale factor. The above scaling factor is also applicable for modeling the tamper radius (r), drop height (H), improvement depth (d_i), crater depth (d_c) and radial distance from tamper center (x) (Eq. 16.2a–e).

$$r_m = \frac{r_p}{N} \tag{16.2a}$$

$$H_m = \frac{H_p}{N} \tag{16.2b}$$

$$(d_i)_m = \frac{(d_i)_p}{N} \tag{16.2c}$$

$$(d_c)_m = \frac{(d_c)_p}{N} \tag{16.2d}$$

$$x_m = \frac{x_p}{N} \tag{16.2e}$$

The base area of tamper (A) ($A = \pi r^2$) used in inducing DC in centrifuge is reduced by N^2 times that of the tamper used in the prototype [Eq. (16.3)], while the volume of crater (V_c) induced in model surface is scaled by a factor of N^3 [Eq. (16.4)]. In addition, the tamper velocity [$v = (2gH)^{0.5}$] at the moment of blow (v) is related to its height of fall (H) and gravitational acceleration (g), and is scaled using Eq. (16.5):

$$\frac{A_m}{A_p} = \frac{\pi r_m^2}{\pi r_p^2} = \frac{1}{N^2} \tag{16.3}$$

$$\frac{(V_c)_m}{(V_c)_p} = \frac{1}{N^3} \tag{16.4}$$

$$\frac{v_m}{v_p} = \sqrt{\frac{2(Ng)H_m}{2gH_p}} = 1 \tag{16.5}$$

The work done by tamper in inducing crater at the soil surface is derived from its kinetic energy (KE) at the onset of tamper blow. By definition, work done is the product of force and displacement, and is scaled by a factor of $1/N^3$ [Eq. (16.6)].

Based on scaling of the tamper velocity and kinetic energy, scale factor for tamper mass (m) can be further derived [Eq. (16.7)].

$$\frac{\mathrm{KE_m}}{\mathrm{KE_p}} = \frac{F_\mathrm{m}(d_\mathrm{c})_\mathrm{m}}{F_\mathrm{p}(d_\mathrm{c})_\mathrm{p}} = \frac{1}{N^3} \tag{16.6}$$

$$\frac{m_\mathrm{m}}{m_\mathrm{p}} = \left[\frac{2(\mathrm{KE})_\mathrm{m}}{v_\mathrm{m}^2}\right]\left[\frac{v_\mathrm{p}^2}{2(\mathrm{KE})_\mathrm{p}}\right] = \frac{1}{N^3} \tag{16.7}$$

As the tamper strikes the soil surface, Rayleigh waves are generated, which spread radially on the ground. The peak ground velocity (PGV) of the soil surface is used for quantifying these waves, which is scaled as in Eq. (16.8) similar to tamper velocity.

$$\frac{(\mathrm{PGV})_\mathrm{m}}{(\mathrm{PGV})_\mathrm{p}} = \frac{v_\mathrm{m}}{v_\mathrm{p}} = 1 \tag{16.8}$$

The relevant scaling laws for modeling DC in centrifuge are summarized in Table 16.2.

Table 16.2 Scaling laws applicable for modeling DC in a geotechnical centrifuge

Parameters	Prototype	Model scale
Cohesion (c) (kPa)	1	1
Angle of internal friction (ϕ) (°)	1	1
Unit weight of the soil (γ) (kN/m^3)	1	[a]N
Relative density of soil (RD) (%)	1	1
Pore water pressure in soil (u) (kPa)	1	1
Seepage time (t_s) (s)	1	$1/N^2$
Coefficient of permeability (k) (m/s)	1	N
Tamper mass (m) (t)	1	$1/N^3$
Tamper radius (r) (m)	1	$1/N$
Tamper drop height (H) (m)	1	$1/N$
Time interval between successive blows (t_i) (min)	1	$1/N$
Time for generation of pore water pressure (t_g) (s)	1	$1/N$
Frequency of blows (f_b) (min^{-1})	1	N
Velocity of tamper (v) (m/s)	1	1
Peak ground acceleration (PGA) (m/s^2)	1	N
Peak ground velocity (PGV) (mm/s)	1	1
Crater depth (d_c) (m)	1	$1/N$
Crater volume (V_c) (m^3)	1	$1/N^3$
Depth of improvement (d_i) (m)	1	$1/N$
Kinetic/potential energy of tamper blow (E) (t-m)	1	$1/N^3$
Momentum of tamper (M) (t-m/s)	1	$1/N^3$

N Gravity level or scale factor
[a]For example, $\gamma_\mathrm{m}/\gamma_\mathrm{p} = N$; m: model; p: prototype

16.3 Design Details of Actuator

An actuator was custom-designed and developed in the present study based on the scaling laws presented in Table 16.2. The model test package and actuator assembly are shown in Fig. 16.3. The developed actuator consists of primarily four different components, referred to as the support system, impactor assembly, tamper—hook

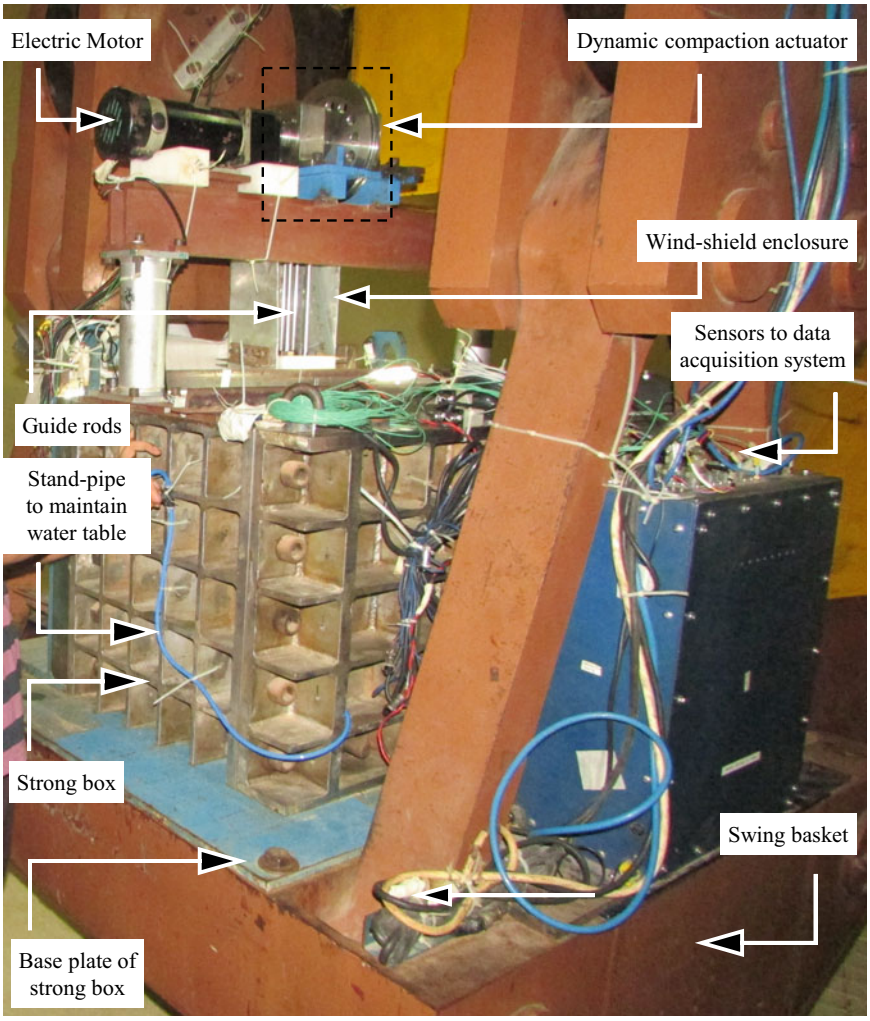

Fig. 16.3 Model test package with DC actuator assembly

arrangement and guiding rod assembly. The support system of the developed actuator consists of three distinctive components, referred to as supporting beam, supporting columns and associated flanges with slot arrangement. The beam has been custom-designed to support the loading transferred by the entire actuator and subsequently transfers the structural load to the supporting columns by a suitably designed nut–screw arrangement. In addition, the presence of supporting columns on either side of the beam component ensures elevation of tamper to a considerable height above the model soil surface in centrifuge, thereby increasing the drop height to the range that is usually adopted in the field. Supporting columns distribute the loads to the strongbox through two properly designed flanges made of 10-mm-thick mild steel plates. Slots provided along the centerline of the flanges enable horizontal shift of the DC assembly, which is advantageous while modeling the effects of variable tamper radii in centrifuge.

The impactor assembly is the fundamental lifting component of the developed in-flight actuator. It is responsible for elevating tamper to a specified height and releasing it under the influence of gravity with the help of four fundamental components, namely drive shaft, sheave, steel hoist rope and a pair of bearing housings. Besides, an assembly of guide rods is provided at the impactor assembly base to ensure vertical alignment of tamper during all stages of centrifuge test. Tamper and hook arrangement are the core components of the tamping module of the in-flight actuator. Three distinctive components, namely base plate, guide shafts and collar, are integrated to constitute the tamper. The base plate is half-circular in shape, as only one-half of circular tamper used in the field was modeled during centrifuge tests. In order to model the effects of variable tamper radii and variable mass of tamper in centrifuge, the base plate is proportioned accordingly to comply with scaling requirements, while keeping guide shafts and collar components unaltered. Hook arrangement consists of two primary components, the hook itself and hook holding block. The guiding rod assembly comprises two individual sets of guiding rods, referred herein as central rods and peripheral rods. The central guiding rods are made to pass through hollow guide shafts and enable linear guidance of tamper. The peripheral guide rods are compactly secured to the bottom surface of impactor assembly. Their primary function is to counter Coriolis acceleration generated during flight.

Additional components associated with the developed actuator include standpipes for maintaining groundwater level, electric motor for providing the mechanical power necessary for rotating the drive shaft, digital camera for recording proceedings of experiment, windshield enclosure to prevent disturbances from artificial air currents above the model soil surface and illumination arrangement in the form of thin strips of LED light. The instrumentation included accelerometers and pore water pressure transducers. The accelerometers are DJB piezoelectric sensors (models: A/23/S and A/23/TS), whereas the pore water pressure transducers are Druck PDCR81 type miniature PPTs (GE make, UK). These miniature Druck PDCR 81 PPTs have been used extensively by researchers

to monitor pore water pressure variations in centrifuge (Muraleetharan and Granger 1999; Ghayoomi et al. 2011; Bhattacherjee and Viswanadham 2018). The data from PPTs were acquired at sampling rate of 10,000 data per sec during DC and at a normal rate of 1 datum per sec before and after inducing DC. The accelerometers were positioned on the soil surface at 0.15, 0.30 and 0.45 m distances from tamper center to measure vertical vibrations (A1_V, A3_V and A5_V) and horizontal vibrations (A2_H, A4_H and A6_H).

16.4 Salient Features of Developed Actuator

The in-flight actuator exhibits the following advantages over existing simulators:

- The actuator is robust and versatile and can be controlled remotely in-flight for replicating DC on geomaterials with variable drop heights, tamper shapes, tamper radii and tamper mass. Thus, the actuator can model the effects of both low-energy and high-energy DC processes adopted in the field within the controlled conditions of a geotechnical centrifuge.
- Adequate measures are taken by providing an assembly of guide rods to counter Coriolis effects in centrifuge and to prevent lateral shift of tamper.
- Another notable advantage of the actuator is its capability to model the time interval between successive drops during DC by regulating the drop frequency through a remotely operated motor. This facilitates monitoring of pore water pressure response in saturated soils subjected to DC.

16.5 Test Procedure and Model Materials

Centrifuge model tests were conducted at 30 gravities using the 4.5-m radius large beam centrifuge available at IIT Bombay, India. Details of the centrifuge facility are summarized briefly in Table 16.3. During discussion, model values have been referred, with corresponding prototype values within parenthesis. Model tests were conducted on loose granular soil deposits of 330 mm (9.9 m) depth subjected to DC under dry and saturated conditions. The model soil used is poorly graded Goa sand (SP) of specific gravity of 2.654, having a permeability of 1.85×10^{-4} m/s at a relative density (R.D.) of 35%. Detailed properties of sand are presented in Table 16.4.

A rigid container with internal dimensions of 720 mm × 450 mm × 410 mm provided with a front transparent perspex plate was used for model preparation and testing (Fig. 16.3). Permanent markers made of thin transparency sheets were pasted at fixed intervals to serve as reference points for subsequent GeoPIV analysis. The sand bed was prepared in a loose dry state at 35% R.D. by adopting the air pluviation technique. Details of model preparation are outlined in Kundu and Viswanadham (2021). Among the two tests conducted (Table 16.5), Model TC1

Table 16.3 Details of the large beam centrifuge facility at IIT Bombay

Sr. no.	Parameters	Details
1	Configuration type	Beam centrifuge
2	Radius	4.5 m (measured up to top surface of the basket from center of the shaft)
3	Radial acceleration range	10–200 g
4	Maximum pay load (at 100 g)	2.5 tons
5	Capacity	250 g-tons
6	Run-up time from 1 to 200 g	6 min
7	Model area	1.00 m × 1.2 m (up to 0.66 m height) 0.76 m × 1.2 m (up to 1.20 m height)

Table 16.4 Summary of properties for Goa sand

Properties	Unit	Soil A (sand)
Specific gravity (G_s)	[a]–	2.654
Sand (0.075–4.75 mm)	%	100
Effective particle size (D_{10})	mm	0.101
Average particle size (D_{50})	mm	0.191
Coefficient of uniformity (C_u)	[a]–	2.065
Coefficient of curvature (C_c)	[a]–	1.117
Maximum void ratio (e_{max})	[a]–	0.94
Minimum void ratio (e_{min})	[a]–	0.63
[b]Cohesion (c')	kPa	0
[b]Friction angle (ϕ')	°	32
[d]Coefficient of permeability at 35% relative density	m/s	[c]1.85×10^{-4}

[a]Not relevant
[b]CU test [35% R.D.]
[c]Average of three tests
[d]Constant head permeability test

Table 16.5 Summary of centrifuge tests conducted in the present study

Test legend	[a]Parameters varied	[a]Constant parameters
TC1–TC2	Depth of groundwater table d_w = Nil, 1.5 m	N = 30, $\gamma_{d,i}$ = 14.22 kN/m^3, m = 20.79 t, r = 1.2 m, H = 10 m, E = 208 t-m, *soil type*: sand

N Gravity level; d_w depth of GWT from soil surface; m mass of tamper; r tamper radius; H drop height; E tamper energy in each blow

corresponded to a dry model, whereas an initial water table was simulated prior to DC for Model TC2. The groundwater table was established in Model TC2 at normal gravity (1 g) by employing the bottom to top flow method. Standpipes connected to the model container ensured maintenance of desired water head at a depth of 50 mm (1.5 m at 30 g) from the model surface. The mass of semicylindrical tamper used in centrifuge tests was 0.385 kg (10.395 t). Due to axial symmetry, only half of the tamper was modeled, thereby replicating a cylindrical tamper of 0.77 kg (20.79 t) mass. An energy level of 7.7 kg-m (208 t-m) was simulated, thereby replicating high-energy DC process. A total of 16 drops were delivered on the soil surface in each test, in view of the marginal increase in improvement depth observed beyond 16 blows, as per the numerical simulations of Gu and Lee (2002). The pore water pressure generation during DC and corresponding vibration levels induced at the ground surface were analyzed based on data recorded by PPTs and accelerometers, whereas the ground improvement induced by DC was ascertained through contours of displacements and volumetric strains.

16.6 Results and Discussion

The interpretation of centrifuge model tests through instrumentation data and GeoPIV analysis on in-flight images are discussed in this section and summarized in Table 16.6.

16.6.1 Crater Profiles Induced by DC

The crater profiles for dry sand (Model TC1) and saturated sand (Model TC2) with increasing distance from tamper center are presented in Fig. 16.4 corresponding to the 1st, 4th, 8th and 16th blows. The maximum crater depth is observed to be about 38 mm (1.15 m) in Model TC1 and 53 mm (1.6 m) in Model TC2. In addition, the

Table 16.6 Summary of centrifuge test results

Test legend	d_w (m)	$d_{i,e}$ (m)	$(d_c)_{max}$ (m)	[b]PGA (g)		[b]PGV (mm/s)	
				Radial	Vertical	Radial	Vertical
TC1	[a]–s	5.59	1.16	0.191	0.284	32.8	18.2
TC2	1.5	5.03	1.58	0.204	0.233	27.0	17.1

All tests were conducted at gravity level of 30 g ($N = 30$)
Note All values are reported in prototype scale
[a]Dry soil sample
[b]Reported after 16th blow at 13.5 m from tamper center
d_w Depth of water table from soil surface; $d_{i,e}$ effective depth of improvement; $(d_c)_{max}$ maximum crater depth; PGA peak ground acceleration; PGV peak ground velocity

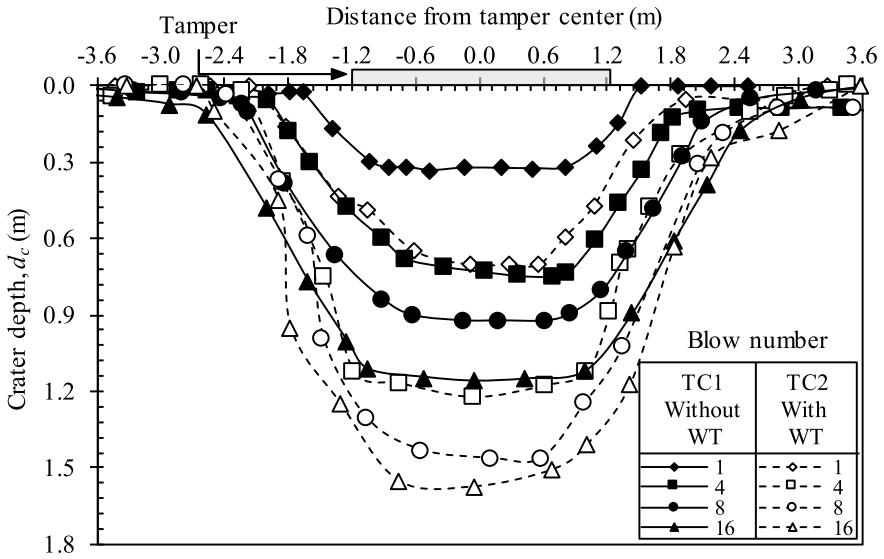

Fig. 16.4 Crater depths for Model TC1 and Model TC2

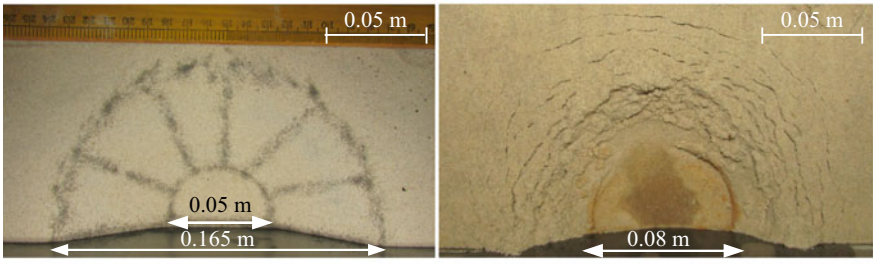

(a) TC1, Dry sand (b) TC2, Sand with water table

Fig. 16.5 Top view of crater induced by DC on various soil types

top view of crater observed during posttest investigations after completion of DC is shown in Fig. 16.5a, b. In general, well-defined crater surfaces are observed in dry soil (Model TC1) (Fig. 16.5a) with considerable collapse of crater boundaries. In comparison, the presence of moisture due to groundwater table in Model TC2 prevented collapse of crater boundaries (Fig. 16.5b), resulting in higher crater depths for the same blow number, as evident from Fig. 16.4.

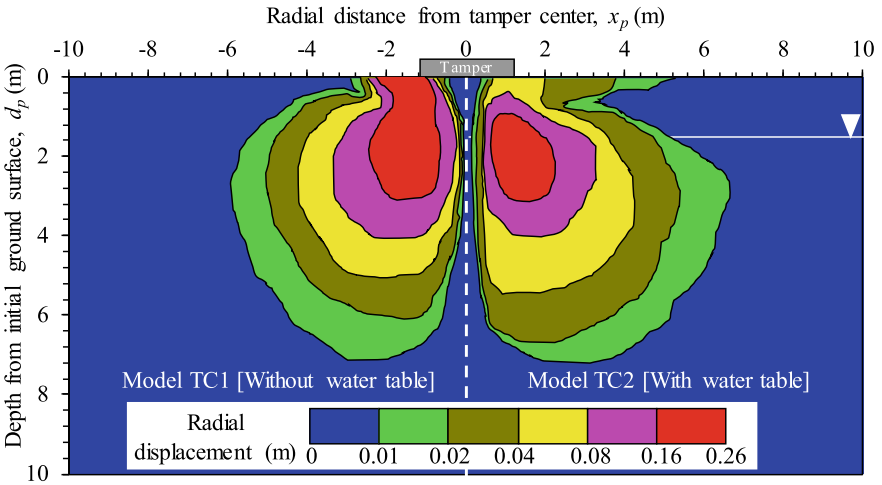

Fig. 16.6 Radial displacement contours for Models TC1 and TC2

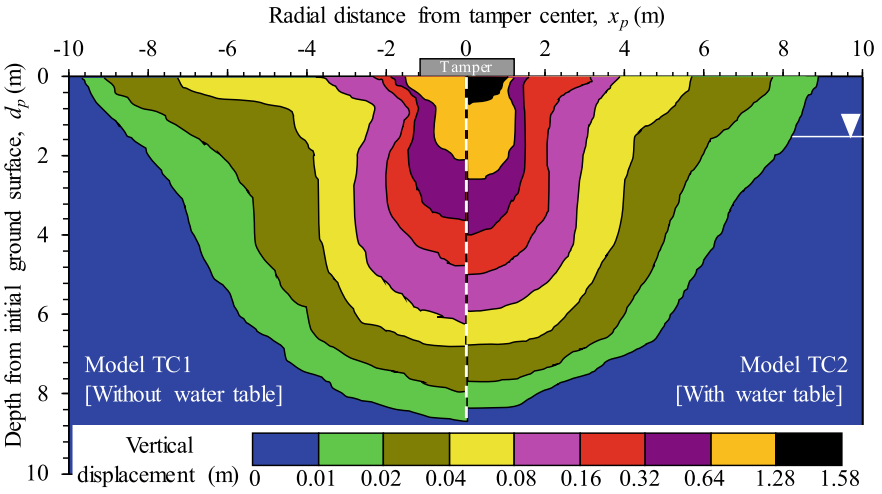

Fig. 16.7 Vertical displacement contours for Models TC1 and TC2

16.6.2 Displacement Contours

The radial and vertical displacement contours of Models TC1–TC2 at the end of 16 blows are presented in Figs. 16.6 and 16.7, respectively. The contours were derived from displacement vectors using GeoPIV software as per the procedure outlined in White et al. (2003). The displacement contours indicated considerable soil movement and associated disturbance in the vicinity of tamper, which reduced with depth

and radial distance from the tamper center. The extent of the disturbed zone was found to be marginally higher in sand with water table (6.6 m in Model TC2) as compared to dry sand (6.0 m in Model TC1), especially in the radial direction. The reason is attributed to lesser resistance provided by saturated sand to soil displacement.

16.6.3 Volumetric Soil Strains

The volumetric strains (ε_v) within soil post-DC were studied for each centrifuge model test as an indication of the extent of ground improvement. The displacement contours shown in Figs. 16.6 and 16.7 were utilized in this regard, together with calculation of volume of individual soil elements before the first blow occurs on the soil surface (V_i), and at a point of time after the final blow (16th blow) is delivered (V_f). Using the above information, R.D. of soil after every blow was ascertained. In the present study, the depth of improvement (d_i) was considered as the thickness of soil strata measured from initial ground surface to a depth below which ΔRD is less than 10% (which corresponds to ε_v = 1.7%). Additionally, an effective depth of improvement ($d_{i,e}$) was defined measured from the base of crater. Numerically, $d_{i,e}$ is equal to difference of depth of improvement and depth of crater, and equal to (d_i–d_c). The volumetric strains (ε_v) plotted in Fig. 16.8 along with d_c, d_i and $d_{i,e}$ indicate marginally higher improvements induced during DC in case of Model TC1 with dry sand ($d_{i,e}$ = 5.59 m) as compared to Model TC2 with water table ($d_{i,e}$ = 5.03 m).

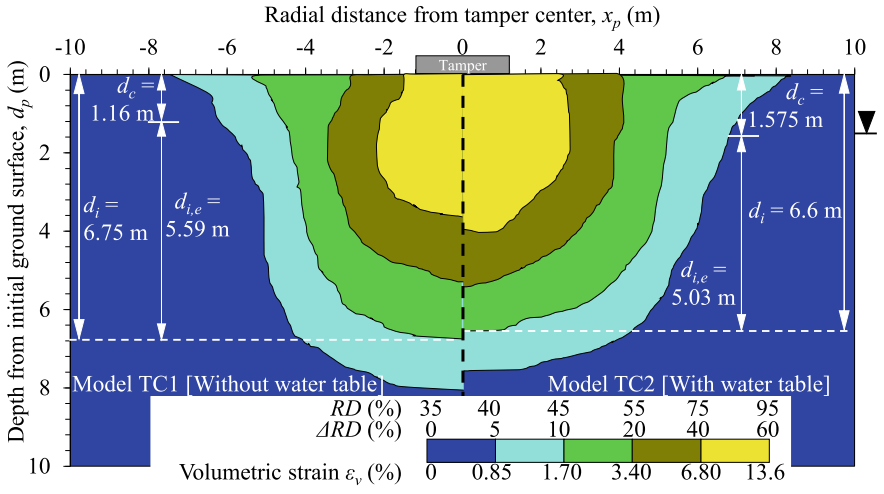

Fig. 16.8 Volumetric strain contours for Models TC1 and TC2

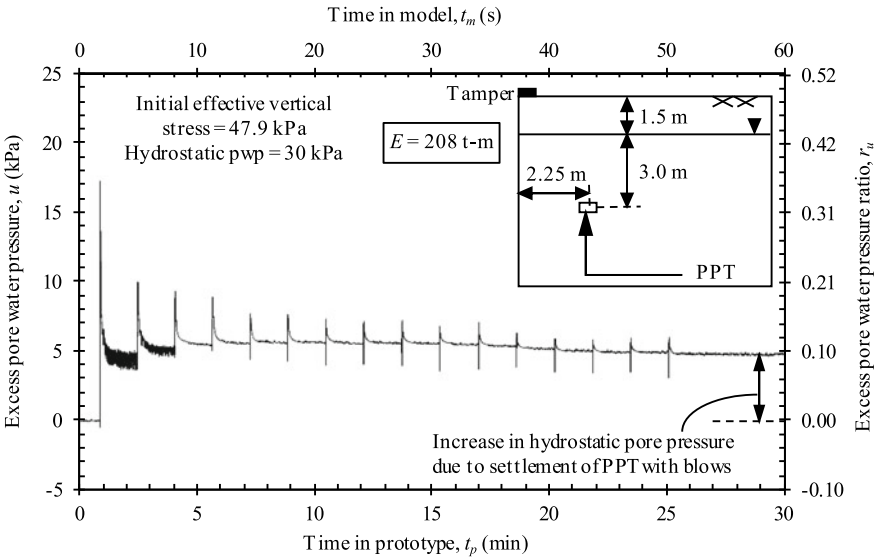

Fig. 16.9 Pore water pressures registered in Model TC2

16.6.4 Pore Water Pressure Developments

The pore water pressures developed in Model TC2 with successive blows are presented in Fig. 16.9 corresponding to a typical PPT placed at 100 mm (3.0 m) below the water table and at a radial distance of 75 mm (2.25 m) from tamper. The peak-induced pore water pressure was observed to be maximum after the 1st blow, which was in the magnitude of 17 kPa. In addition, the excess pore water pressure ratio (r_u) defined as the ratio between excess pore pressure and the total overburden pressure is presented in Fig. 16.9 as a measure of liquefaction potential of the soil. The peak r_u value was about 0.40 in Model TC2. Higher magnitudes of r_u beyond the observed limits could not be captured during centrifuge tests to prevent damage of PPTs placed close to the point of tamper drop.

16.6.5 Ground Vibrations Associated with DC

The peak ground accelerations (PGAs) and peak ground velocities (PGVs) induced during DC were investigated in the study based on data recorded by accelerometers.

The accelerometer data at the end of 4th blow and 16th blow are presented in prototype dimensions in Fig. 16.10a to analyze the PGA induced during tamper blows. The magnitude of PGA after 16th blow in dry sand [Model TC1] was 45 g (1.5 g) [radial] and 37 g (1.23 g) [vertical], respectively, and that in case of

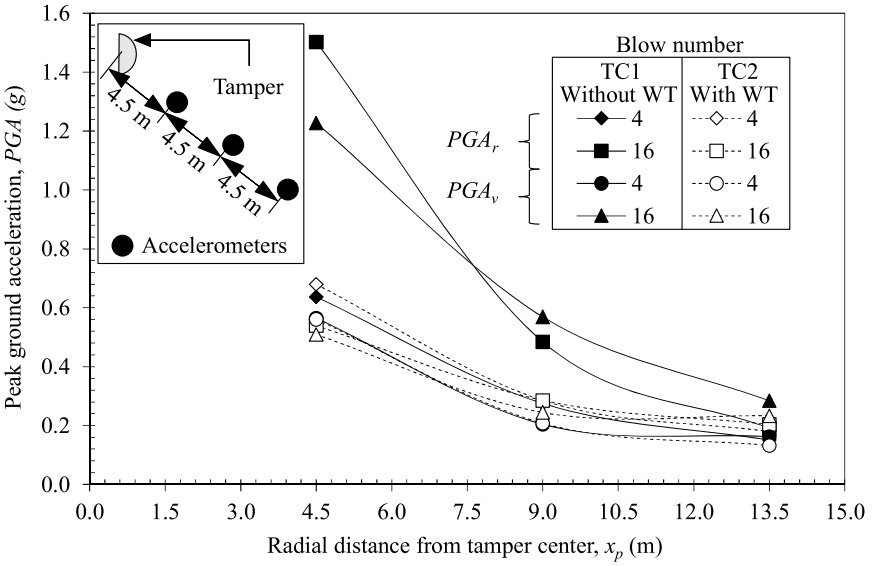

(a) Peak ground accelerations (PGA) induced during DC

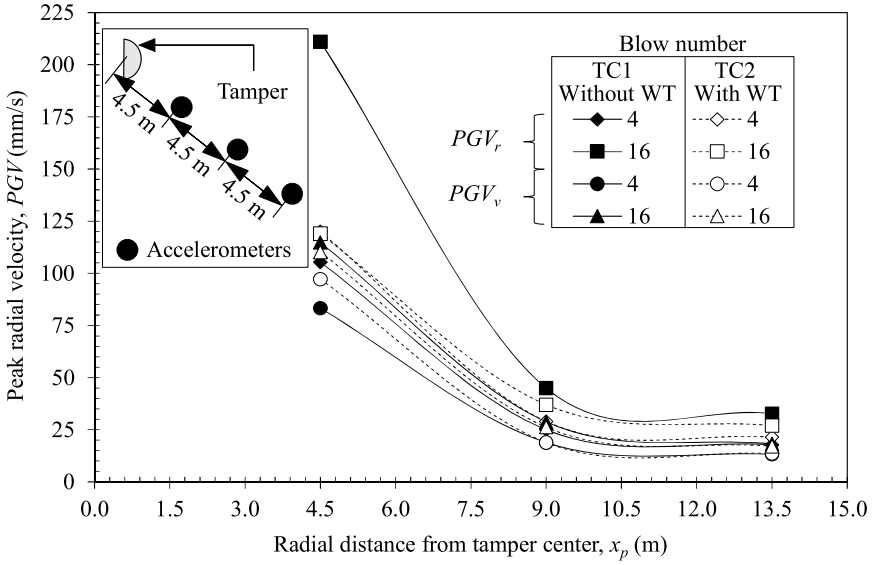

(b) Peak ground velocities (PGV) induced during DC

Fig. 16.10 Ground vibrations associated with DC

saturated sand [Model TC2] was about 20.4 g (0.68 g) [radial] and 16.8 g (0.56 g) [vertical]. In the next step, the ground velocities induced during DC were evaluated by integrating the area under the acceleration–time plots with the progress of DC. The resultant PGV values after 4th blow and 16th blow are presented in Fig. 16.10b. The peak radial velocity near tamper after 16th blow (PGV_r) was about 211 and 120 mm/s, respectively, in Model TC1 (dry) and Model TC2 (saturated). The corresponding peak vertical velocity (PGV_v) was about 112 mm/s in Model TC1 (dry) and Model TC2 (saturated). Thus, it can be observed that the radial component of vibrations was generally higher than corresponding vertical ones induced by DC. Further, the PGA and PGV induced during DC decreased in the presence of water table owing to damping effects in saturated soil.

16.7 Conclusions

The present paper discusses the development and key features of an actuator for simulating DC on geomaterials within the high-gravity environment prevailing in a geotechnical centrifuge. The governing laws, components of the actuator, model materials, model test package and instrumentation details are discussed explicitly. The actuator was employed to replicate high-energy DC process on sand with and without water table using the 4.5-m radius beam centrifuge at IIT Bombay, India. The primary findings are summarized herein:

- Based on GeoPIV analysis of selected images captured in-flight during experimentation, crater profiles, contours of soil displacement and volumetric strains were plotted to quantify the ground improvement induced by DC. The improvement depth was found to be comparable for both models, with marginally higher values in dry sand.
- The pore pressure magnitudes in sand with groundwater table peaked after 1st blow in tamper vicinity, which reduced gradually with successive blows.
- The corresponding ground vibrations induced by DC interpreted in terms of PGA and PGV values indicated that the radial component was higher than corresponding vertical ones. Further, the PGA and PGV induced during DC increased with successive blows and decreased in the presence of water table.

Based on the above, it can be inferred that the actuator can effectively model DC in dry and saturated soils within a geotechnical centrifuge. In addition, the developed actuator can provide an insight into the response of diverse field deposits subjected to DC, including dumped fills, hydraulically deposited fills, peats, collapsible soils, municipal solid waste landfills, dredged soils, reclaimed fills and so on.

References

Bhattacherjee D, Viswanadham BVS (2018) Design and performance of an inflight rainfall simulator in a geotechnical centrifuge. Geotech Test J ASTM 41(1):72–91

Bo MW, Na YM, Arulrajah A, Chang MF (2009) Densification of granular soil by dynamic compaction. Ground Improv 162(3):121–132

Feng SJ, Shui WH, Tan K, Gao LY, He LJ (2011) Field evaluation of dynamic compaction on granular deposits. J Performance Constr Facilities ASCE 25(3):241–249

Ghayoomi M, McCartney J, Ko HY (2011) Centrifuge test to assess the seismic compression of partially saturated sand layers. Geotech Test J ASTM 34(4):1–11

Gu Q, Lee FH (2002) Ground response to dynamic compaction of dry sand. Géotechnique 52 (7):481–493

Kundu S, Viswanadham BVS (2018) Numerical studies on the effectiveness of dynamic compaction using shear wave velocity profiling. Indian Geotech J Springer 48(2):305–315

Kundu S, Viswanadham BVS (2020) Numerical modelling of dynamic compaction induced settlement of MSW landfills. Int J Geomech ASCE 20(8):04020125–1:12

Kundu S, Viswanadham BVS (2021) Design and development of an in-flight actuator for modelling dynamic compaction in a geotechnical centrifuge. Geotech Test J ASTM 44(4):28 (published ahead of print)

Leonards GA, Cutter WA, Holtz RD (1980) Dynamic compaction of granular soil. J Geotech Eng ASCE 106(1):35–44

Lukas RG (1986) Dynamic compaction for highway construction, vol. 1: design and construction guidelines. Federal Highway Administration, Report No. RD-86/133, Washington D.C., pp 204–219

Lukas RG (1995) Geotechnical engineering circular no. 1—dynamic compaction. U. S. Federal Highway Administration, Report No.- FHWA-SA-95–037, Washington D.C.

Lutenegger AJ (1986) Dynamic compaction in friable loess. J Geotech Geoenviron Eng ASCE 112 (6):663–667

Madabhushi G (2014) Centrifuge modeling for civil engineers. CRC Press, USA

Mayne PW, Jones JS (1983) Impact stress during dynamic compaction. J Geotech Eng ASCE 109 (10):1342–1347

Mayne PW, Jones JS, E'Dinas DC (1984) Ground response to dynamic compaction. J Geotech Eng ASCE 110(6):757–774

Menard L, Broise Y (1975) Theoretical and practical aspects of dynamic consolidation. Géotechnique 25(1):3–18

Muraleetharan K, Granger K (1999) The use of miniature pore pressure transducers in measuring matric suction in unsaturated soils. Geotech Test J ASTM 22(3):226–234

Rollins KM, Rogers GW (1994) Mitigation measures for small structures on collapsible soils. J Geotech Eng ASCE 120(9):1533–1553

Schofield AN (1980) Cambridge geotechnical centrifuge operations. Géotechnique 30(3):227–268

Taylor RN (1995) Centrifuges in modelling: principles and scale effects. In: Taylor RN (ed) Geotechnical centrifuge technology. Blackie Academic and Professional (pubs.), Glasgow, UK

White DJ, Take WA, Bolton MD (2003) Soil deformation measurement using particle image velocimetry (PIV) and photogrammetry. Géotechnique 53(7):619–631

Yee K, Ooi TA (2010) Ground Improvement—a green technology towards a sustainable housing, infrastructure and utilities developments in Malaysia. Geotech Eng J SEAGS AGSSEA 41 (3):1–20

Zekkos D, Kabalan M, Flanagan M (2013) Lessons learned from case histories of dynamic compaction at municipal solid waste sites. J Geotech Geoenviron Eng ASCE 39(5):738–751

Zou WL, Wang Z, Yao ZF (2005) Effect of dynamic compaction on placement of high-road embankment. J Performance Constr Facilities ASCE 19(4):316–323